Spin-polarized low-density neutron matter

Alexandros Gezerlis

Spin-polarized low-density neutron matter

Alexandros Gezerlis

Department of Physics, University of Washington, Seattle, Washington, 98195, USA

Low-density neutron matter is relevant to the study of neutron-rich nuclei and neutron star crusts. Unpolarized neutron matter has been studied extensively over a number of decades, while experimental guidance has recently started to emerge from the field of ultracold atomic gases. In this work, we study population-imbalanced neutron matter (possibly relevant to magnetars and to density functionals of nuclei) applying a Quantum Monte Carlo method that has proven successful in the field of cold atoms. We report on the first *ab initio* simulations of superfluid low-density polarized neutron matter. For systems with small imbalances, we find a linear dependence of the energy on the polarization, the proportionality coefficient changing with the density. We also present results for the momentum and pair distributions of the two fermionic components.

I. INTRODUCTION

The inner crust of a neutron star is widely considered to be composed of a lattice of neutron-rich nuclei along with a gas of neutrons and electrons. The gas of neutrons is expected to be superfluid at weak to intermediate coupling. Thus, low-density neutron matter is intrinsically connected to the strongly coupled fermion many-body problem, necessitating accurate calculations (or simulations). Low-density neutron matter is of relevance to the static and dynamic properties of the neutron star crust, which can lead to observable behavior. [1–3] Outside the observational realm, neutron matter computations also hold significance in the context of traditional nuclear physics: equation of state results at densities close to the nuclear saturation density have been used for some time to constrain Skyrme and other density functional approaches to heavy nuclei, while the density-dependence of the $^1S_0$ gap in low-density neutron matter has also been used to constrain Skyrme-Hartree-Fock-Bogoliubov treatments in their description of neutron-rich nuclei [4]. The potential significance of such calculations has led to a series of publications on the equation of state of low-density neutron matter over the last few decades. [5–16]

Parallel developments in a separate field of physics have recently provided new insight as well as the promise of direct experimental constraints: experiments with ultracold atomic gases of fermions are now being carried out in a number of labs around the world. In some cases, atomic gases in non-elongated traps contain sufficiently many particles that the local-density approximation is valid. As a result, such experiments can measure the energy [17, 18] and pairing gap [19, 20] of homogeneous strongly interacting matter. For cold fermionic atoms, the two-particle interaction can be directly tuned using a magnetic field through so-called Feshbach resonances to produce a specific scattering length a, while the effective range r_e between the atoms is considerably smaller than the average interparticle distance, and thus essentially zero. These conditions are analogous to low-density neutron matter, where the particle-particle interaction has a scattering length which is considerable, ≈ -18.5 fm, and is therefore larger than the average interneutron spacing. On the other hand, cold atoms and low-density neutron matter are clearly distinct systems: first, for neutron matter the effective range is much smaller than the scattering length, $r_e \approx 2.7$ fm, so $|r_e/a| \approx 0.15$, but only at very low densities is the effective range much smaller than the interparticle spacing. Second, the neutron-neutron (NN) interaction is not strictly limited to s-waves, implying a complicated spin dependence. Third, three-neutron interactions (NNN) are in principle also present. The last two points can be remedied if one studies relatively low-densities, i.e. at most an order of magnitude smaller than the nuclear saturation density. The first point might be addressed in the framework of cold atomic experiments in the future: it may be possible to use narrow and wide resonances in cold atoms to study this experimentally.[21]

The above discussion is limited to unpolarized neutron matter, i.e. to the case of two species of neutrons, conventionally called spin-up ($\uparrow$) and spin-down ($\downarrow$), with equal populations. However, the general case of imbalanced systems has also been studied extensively: limiting ourselves for the moment to neutron matter, calculations of the magnetic susceptibility have been appearing consistently since the discovery of pulsars. [22] Given that the magnitude of the pairing gap is approximately 1 MeV, a magnetic field in a neutron star crust would have to be larger than $10^{16} - 10^{17}$ G to polarize neutron matter. The question of spin-polarized neutron matter is thus in principle relevant to objects known as magnetars, which have surface magnetic fields of $10^{14} - 10^{15}$ G. Thus, the promise of observational insight into these objects has led a number of theoretical groups to study spin-polarized neutron matter and the associated question of a possible ferromagnetic instability at large density. [23–29]

In this work, we take a step back and address neutron matter with a finite spin-polarization (population imbalance) *at low density*. This system is relevant to neutron star observations: in a realistic neutron-star crust polarization may appear at lower densities than for infinite matter. For example, the spin-orbit splitting around a large nucleus might help favor polarization at a lower

magnetic field than would be required for the bulk. Furthermore, our results could also be used as an input to or benchmark for phenomenological theories of terrestrial nuclei. On a different note, as already mentioned, the region of low-density is close to the physics of cold atoms, since there the NN interaction is simpler and the NNN interaction is minimal. Thus, we can use approaches already verified in the laboratory with ultracold atomic gases. Importantly, we use a Quantum Monte Carlo (QMC) method which has been applied, in previous works, to polarized cold atomic systems, [30, 31] as well as to unpolarized cold atoms and neutron matter [32–34]. Our earlier works were consistent both with experimental measurements and with the analytically known behavior of the energy and the gap at vanishingly small coupling.[35, 36] We extend this QMC method appropriately, allowing us to study spin-polarized superfluid neutron matter and therefore provide the first benchmark calculation of this system using an *ab initio* microscopic simulation approach.

In such systems, it is conventional to use the following measure of the population imbalance:

$$P = \frac{N_\uparrow - N_\downarrow}{N_\uparrow + N_\downarrow} \tag{1}$$

where $N_\uparrow$ and $N_\downarrow$ are the numbers of spin-up and spin-down particles, respectively, and P is called the polarization. The regime of large polarization is related to a question that has a long history in the framework of the BCS theory. In the BCS approach, superfluidity arises from the pairing of particles of different spin occupying states of opposite momenta near the Fermi surface. In the case of spin imbalance, the Fermi surfaces of the two components no longer coincide, making pairs with zero total momentum difficult to form. At some finite polarization, the gap between the two Fermi surfaces becomes so large that the system undergoes a quantum phase transition to a normal state (this is known as the Chandrasekhar-Clogston limit).

Our aim in this work is to provide quantitatively reliable results for superfluid low-density neutron matter. We therefore limit our simulations to small polarizations, $P < 0.1$, exploring the regime where pairing is energetically stable. We calculate ground-state energies at different total number densities ($\rho = (N_\uparrow + N_\downarrow)/L^3$), more specifically at $\rho_1 = 6.65 \times 10^{-4}$, $\rho_2 = 2.16 \times 10^{-3}$, and $\rho_3 = 5.32 \times 10^{-3}$ fm^{-3}. To put these densities into perspective we can compare them to nuclear matter saturation density: they are $0.41, 1.35$, and 3.32 percent, respectively, of $\rho_0 = 0.16$ fm^{-3}. At each total density, we study the cases of $35 + 33$, $37 + 33$, and $39 + 33$ particles (see below). We also compute the momentum distributions and pair-distribution functions for the two different components.

II. QUANTUM MONTE CARLO

A. Hamiltonian

As pointed out in the Introduction, we do not need to include NNN interactions, since we are interested in a density regime where these are quite small. Thus, we use the following non-relativistic Hamiltonian:

$$\mathcal{H} = \sum_{k=1}^{N}(-\frac{\hbar^2}{2m}\nabla_k^2) + \sum_{i,j} v_4(r_{ij}) , \tag{2}$$

where $N = N_\uparrow + N_\downarrow$ is the total number of particles. The full neutron-neutron interaction is complicated, having one-pion exchange at large distances, an intermediate range spin-dependent attraction by two-pion exchange, and a short-range repulsion. As already discussed, however, in dilute neutron matter the dominant contributions come from the opposite-spin pairs, and specifically from the scattering length and the effective range, along with a short-range repulsive core which is important so as to avoid a collapse to a higher-density state

In this work we are including an excess of neutrons of one species. Thus, it is also significant to take into account the same-spin interactions in Eq. (2), which we do by using the interaction introduced in Ref. [34]. This interaction includes a propagator (see next subsection) in which all opposite-spin pairs interact through the $^1S_0$ channel of the Argonne v18 (AV18) [37] potential, which fits s-wave nucleon-nucleon scattering very well at both low- and high-energies. Thus, in what follows, for the purposes of the evolution the spins are considered to be "frozen", with the majority species being called $\uparrow$ and the minority species being called $\downarrow$. We explicitly include the p-wave interactions in the same-spin pairs, and perturbatively correct the $S = 1, M_S = 0$ pairs to the correct p-wave interaction. We use the AV4$'$ potential to determine the p-wave interactions.[38].

Since we're studying neutrons, the AV4$'$ interaction can be written as follows:

$$v_4(r) = v_c(r) + v_\sigma(r)\boldsymbol{\sigma}_1 \cdot \boldsymbol{\sigma}_2, \tag{3}$$

which in the case of the $S = 0$ singlet pairs gives:

$$v_S(r) = v_c(r) - 3v_\sigma(r) . \tag{4}$$

In turn, the contribution from $S = 1$ (triplet) pairs has the form:

$$v_P(r) = v_c(r) + v_\sigma(r) . \tag{5}$$

The same-spin potential contribution is small, but as the population imbalance increases it also increases accordingly (see section III A). While still keeping the potential of Eq. (4) in the propagator of our QMC method for the opposite-spin pairs, we have introduced a perturbative correction by writing Eq. (3) in terms of the Majorana exchange operator, which exchanges the positions leaving the spins unaffected:

$$v_4(r) = v_c(r) + v_\sigma(r)(-2P^M - 1) \tag{6}$$

B. Variational and Green's Function Monte Carlo

The first step in our microscopic simulation is a Variational Monte Carlo (VMC) calculation. Variational Monte Carlo is a relatively simple combination of classical Monte Carlo and the variational (Rayleigh-Ritz) method; it was first used by McMillan in the 1960s. It is based on a variational trial wave function Ψ_V that is a reasonably good approximation of the true ground-state wave function. It contains variational parameters that in principle should allow one to approach the true wave function (see the next subsection for more details). A VMC calculation uses Monte Carlo integration to minimize the expectation value of the Hamiltonian:

$$\langle H \rangle_{VMC} = \frac{\int d\mathbf{R} \Psi_V(\mathbf{R}) H \Psi_V(\mathbf{R})}{\int d\mathbf{R} |\Psi_V(\mathbf{R})|^2} \geq E_0 \ , \qquad (7)$$

thus optimizing the variational wave function Ψ_V. The fact that it is relatively easy to perform a VMC simulation allows us to examine various possibilities in placing the excess particles in different momentum states.

It is customary to use the output configurations of a Variational Monte Carlo calculation as input to a more extensive calculation using the method known as Green's Function Monte Carlo (GFMC). This method works by projecting out the exact, lowest-energy eigenstate Ψ_0 from a trial (variational) wave function Ψ_V by treating the Schrödinger equation as a diffusion equation in imaginary time τ and stochastically evolving the variational wave function for a "sufficiently" long time.

The evolution operator e^{-iHt} becomes $e^{-H\tau}$ in imaginary time, commonly written as $e^{-(H-E_T)\tau}$, where the E_T is called the trial energy. Applying this operator to the variational wave function and expanding in terms of the complete set of eigenstates gives:

$$\begin{aligned}\Psi(\tau) &= e^{-(H-E_T)\tau}\Psi_V = \sum_i \alpha_i e^{-(E_i-E_T)\tau}\Psi_i \\ &= \alpha_0 e^{-(E_0-E_T)\tau}\Psi_0, \quad \lim \tau \to \infty \ . \end{aligned} \qquad (8)$$

The GFMC technique is implemented by discretizing τ and expressing the imaginary-time propagator as

$$e^{-(H-E_T)\tau} = \prod_n e^{-(H-E_T)\triangle\tau} \ , \qquad (9)$$

where $\tau = n\triangle\tau$. If we now define the short-time Green's function by:

$$G(\mathbf{R},\mathbf{R}') = \langle \mathbf{R}|e^{-(H-E_T)\triangle\tau}|\mathbf{R}'\rangle \ , \qquad (10)$$

where $\mathbf{R}$ is the configuration vector $\mathbf{R} = (\mathbf{r}_1, \mathbf{r}_2 \ldots \mathbf{r}_N)$ of $3N$ dimensions, then we can use it to calculate the evolved $\Psi(\tau)$ starting from a set of VMC configurations. The short-time Green's function can be conveniently approximated using the Trotter-Suzuki formula:

$$\begin{aligned}G(\mathbf{R},\mathbf{R}') &\approx e^{-V(\mathbf{R})\frac{\triangle\tau}{2}}\langle \mathbf{R}|e^{-T\triangle\tau}|\mathbf{R}'\rangle e^{-V(\mathbf{R}')\frac{\triangle\tau}{2}}e^{E_T\triangle\tau} \\ &= e^{-(V(\mathbf{R})+V(\mathbf{R}')-2E_T)\frac{\triangle\tau}{2}}\langle \mathbf{R}|e^{-T\triangle\tau}|\mathbf{R}'\rangle \end{aligned} \ (11)$$

which is accurate to order $(\Delta\tau)^2$.

To avoid the fermion-sign problem, we impose what is known as the "fixed-node approximation". A fixed-node simulation leads to a wave function Ψ_0 that is the lowest-energy state with the same nodes as the trial wave function Ψ_V. The resulting energy E_0 is an upper bound to the true ground-state energy. Thus, if one chooses the variational wave function so that it includes a number of parameters, [32] these parameters can be optimized to give the best approximation to the ground-state wave function (see next subsection).

C. Trial wave function

In these VMC and GFMC calculations there is a need to express the wave function of the system in terms of specific coordinate-space states. To this effect, we use a finite number N of particles with Born-von Karman (periodic) boundary conditions in a cubic box of volume L^3, and N is chosen to be large enough so that the system can be assumed to be in the thermodynamic limit. For neutron matter, this was shown to be approximately 66 particles in Ref. [33]. Using a Cartesian coordinate system, the quantized plane waves $e^{i\mathbf{k_n}\cdot\mathbf{r}}$ will have momentum vectors of the following discrete form:

$$\mathbf{k_n} = \frac{2\pi}{L}(n_x, n_y, n_z) \ , \qquad (12)$$

where the n_x, n_y, n_z are integers. The shell number I is defined such that $I = n_x^2 + n_y^2 + n_z^2$. Thus, there is only 1 possible combination of the n_x, n_y, n_z that gives $I = 0$, 6 combinations that produce $I = 1$, 12 combinations that lead to $I = 2$ and so on. Neutrons are spin one-half fermions, therefore if we address equal populations for the two components the system has a closed-shell structure when $N = 2, 14, 38, 54, 66, \ldots$.

The simplest possible approximation (which, strictly speaking, is applicable only to the case of closed shells) that can be used for the input variational wave function is to describe the particles as being in a free Fermi gas. This approach assumes no correlations in the wave function and is equivalent to having a product of two Slater determinants, one for spin-up and one for spin-down:

$$\Phi_S(\mathbf{R}) = D_\uparrow D_\downarrow. \qquad (13)$$

The single-particle states in the Slater determinants are $\phi_n(r_k) = e^{i\mathbf{k_n}\cdot\mathbf{r}_k}/L^{3/2}$.

Another choice for $\Phi(\mathbf{R})$, one which can also describe pairing, is the well-known BCS wave function $\Phi_{BCS}(\mathbf{R})$ in its form for fixed particle number (which reduces to the Slater case under specific conditions). This choice is agreeable for both physical reasons (it reflects the fact that fermions with an attractive interaction can form Cooper pairs in the ground state) and mathematical reasons (*unlike* the Slater wave function, it has nodal surfaces which can be varied so as to minimize the fixed-node

GFMC energy). Furthermore, a computationally appealing aspect of this wave function is the fact that it can be written down as a determinant. [39]

In this formalism, a general wave function with n pairs, u spin-up and d spin-down unpaired particles can be written as:

$$\Phi_{\text{BCS}}(\mathbf{R}) = \mathcal{A} \left\{ [\phi(r_{11'})...\phi(r_{nn'})] \left[\psi_{1\uparrow}(\mathbf{r}_{n+1})...\psi_{u\uparrow}(\mathbf{r}_{n+u}) \right] \left[\psi_{1\downarrow}(\mathbf{r}_{(n+1)'})...\psi_{d\downarrow}(\mathbf{r}_{(n+d)'}) \right] \right\} \ . \tag{14}$$

The unpaired particles are placed in $\psi_{i\uparrow}$ and $\psi_{j\downarrow}$ single-particle states. We can write this wave function as the determinant of an $M \times M$ matrix where $M = n + u + d$. In this work, we are interested in the case of a "gapless superfluid" which for polarized neutrons translates to 33 opposite-spin pairs along with an excess of unpaired particles of one species. When we have 2 extra spin-up particles, the corresponding matrix is written as follows:

$$\begin{pmatrix} \phi(r_{1,1'}) & \phi(r_{1,2'}) & ... & \phi(r_{1,33'}) & \psi_{1\uparrow}(\mathbf{r}_1) & \psi_{2\uparrow}(\mathbf{r}_1) \\ \phi(r_{2,1'}) & \phi(r_{2,2'}) & ... & \phi(r_{2,33'}) & \psi_{1\uparrow}(\mathbf{r}_2) & \psi_{2\uparrow}(\mathbf{r}_2) \\ \vdots & \vdots & \vdots\vdots\vdots & \vdots & \vdots & \vdots \\ \phi(r_{35,1'}) & \phi(r_{35,2'}) & ... & \phi(r_{35,33'}) & \psi_{1\uparrow}(\mathbf{r}_{35}) & \psi_{2\uparrow}(\mathbf{r}_{35}) \end{pmatrix} \tag{15}$$

The pairing function $\phi(r)$ is a sum over the momenta compatible with the periodic boundary conditions. In the BCS theory the pairing function is:

$$\phi(r) = \sum_{\mathbf{n}} \frac{v_{\mathbf{k_n}}}{u_{\mathbf{k_n}}} e^{i\mathbf{k_n}\cdot\mathbf{r}} = \sum_{\mathbf{n}} \alpha_n e^{i\mathbf{k_n}\cdot\mathbf{r}} \ , \tag{16}$$

and here it is parametrized with a short- and long-range part as in Ref. [32]:

$$\phi(\mathbf{r}) = \tilde{\beta}(r) + \sum_{\mathbf{n}, \ I \leq I_C} \alpha_I e^{i\mathbf{k_n}\cdot\mathbf{r}} \ , \tag{17}$$

We choose the single-particle states, $\psi_{i\uparrow}$, to be plane waves so as to ensure momentum conservation. We pick their momentum by checking values near the minimum (at each density) of the quasiparticle dispersion. The latter is calculated using the odd-even energy staggering:

$$\Delta = E(N+1) - \frac{1}{2} \left[E(N) + E(N+2) \right] \ , \tag{18}$$

where N is an even number of particles. At each density, the minimum of the dispersion lies at a different momentum.[34] As already mentioned, we used VMC to place the particles at different momentum states. For very small polarizations, the minimum system energy is expected to be identical to the minimum of the dispersion, which follows from adding only one extra particle. This is indeed the result we find, the only exceptions appearing at density ρ_3 and particle numbers of $39+33$ and higher (see below).

In practice, we also include Jastrow (correlation) terms in the variational wave function:

$$\Psi_V = \prod_{i \neq j} f_P(r_{ij}) \prod_{i' \neq j'} f_P(r_{i'j'}) \prod_{i,j'} f(r_{ij'}) \Phi_{\text{BCS}}(\mathbf{R}) \tag{19}$$

where the unprimed (primed) indices refer to spin-up (spin-down) particles. The Jastrow parts are taken from

a lowest-order-constrained-variational method [40] calculation described by a Schrödinger-like equation:

$$-\frac{\hbar^2}{m}\nabla^2 f(r) + v(r)f(r) = \lambda f(r) \tag{20}$$

for the opposite-spin $f(r)$ and

$$-\frac{\hbar^2}{m}\nabla^2 f(r) + v(r)f(r) + \frac{2\hbar^2}{mr^2}f(r) = \lambda f(r) \tag{21}$$

for the same-spin $f_P(r)$. Since the $f(r)$ and $f_P(r)$ we use are nodeless, they do not affect the final result apart from reducing the statistical error. Since we are using the fixed-node approximation, we know that the result we obtain for one set of pairing function parameters in Eq. (17) will be an upper bound to the true ground-state energy of the system. The parameters are optimized in the full GFMC calculation as in previous works [32, 33], providing the best possible nodal surface, in the sense of lowest fixed-node energy, for that form of trial function. As mentioned in section II B, this upper-bound property allows us to get as close as possible to the true ground-state energy of the spin-polarized superfluid system.

III. RESULTS

A. Equation of state

We first address the energy of spin-polarized low-density neutron matter versus polarization. We have studied three total densities $\rho_1 = 6.65 \times 10^{-4}$, $\rho_2 = 2.16 \times 10^{-3}$, and $\rho_3 = 5.32 \times 10^{-3}$ fm^{-3}. A smaller density would correspond to neutron matter that is closer to the neutron star surface, which in turn implies a smaller magnetic field, and is thus less likely to be polarized. Also, lower density is more difficult to propagate in imaginary

TABLE I: Results for the ground-state energy divided with the total number of particles for two species of neutrons interacting via an AV4′ potential at $\rho_3 = 5.32 \times 10^{-3}$ fm^{-3}.

$N_\uparrow + N_\downarrow$	E_{full} [MeV]	$E_{\uparrow\uparrow}$ [keV]	$E_{\downarrow\downarrow}$ [keV]
33+33	2.133(1)	11.4(1)	11.3(1)
35+33	2.178(2)	12.2(1)	10.7(1)
37+33	2.230(2)	12.7(1)	10.0(1)
39+33	2.286(2)	13.8(2)	9.6(1)

time to a satisfactory accuracy level, given that lower density leads to larger inverse energy and therefore longer propagation. Reversely, we do not study even larger densities because then we would have to include 3-body interactions in our approach. For pure neutron matter this would imply, first, going away from firm experimentally constrained interactions (threee-neutron interactions are commonly fit to $N = Z$ nuclei) and, second, the necessity of using spin-isospin dependent wave functions, therefore disallowing the use of approximately 70 particles and thus the simulation of the thermodynamic limit in the framework of a variational *ab initio* approach. Furthermore, larger densities would imply that the aforementioned perturbative correction in the propagator (see section II A) would break down. This latter point provides yet another reason why only small polarizations are studied: for these calculations to be quantitatively reliable, the number of opposite-spin pairs should not stray too much from the "canonical" $33 + 33$ case. Thus, for each of the three densities, we address the cases of $35+33$, $37 + 33$, and $39 + 33$ particles. For the case of the largest density we have also examined $41 + 33$ and $43 + 33$ particles (i.e. up to nearly double the polarization), finding the same overall trend.

In most works on polarized neutron matter, the dependence of energy on polarization is taken to be quadratic.[23–29] However, these works address dense neutron matter, in which the $^1S_0$ pairing has already reached gap closure, in the presence of a strong magnetic field. In other words, most works in the literature study normal matter, in which an isolated spin-flip only impacts particles near their respective Fermi surfaces. In this work we study low-density polarized neutron matter, implying that superfluidity plays an important role: flipping a spin is equivalent to breaking a pair. Thus, the pairing gap plays a decisive role in producing the polarized state. Our results for the energy versus polarization exhibit a linear trend:

$$\frac{E}{N}(\rho, P) = \frac{E}{N}(\rho, 0) + \alpha(\rho)P \qquad (22)$$

similarly to the case of ultracold atomic gases at unitarity [30], where Quantum Monte Carlo calculations found a linear dependence of the energy on polarization at small population imbalances.

In this connection, it is relevant to examine the in-
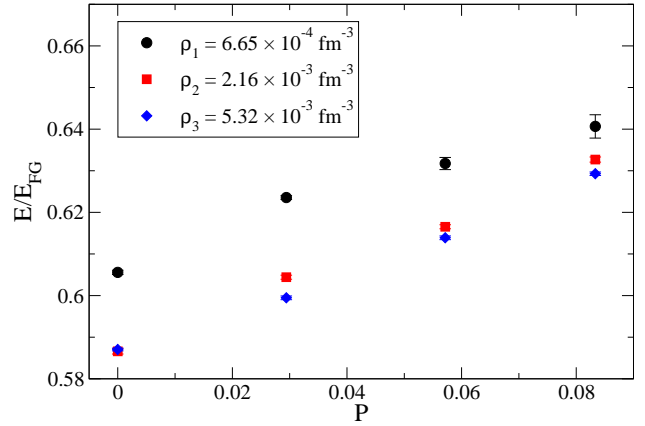

FIG. 1: (color online) Ground-state energy per particle (in units of the free Fermi gas energy) for spin-polarized neutron matter. Shown are QMC results at three different total densities. The overall trend is linear, the slope depending on the density.

teraction between (polarized) quasiparticles. Summing single-particle excitation energies (taken from Ref. [34]) for particles that are placed at the appropriate minimum momentum in Eq. (12) we find that the full Quantum Monte Carlo results are thus approximately reproduced. This implies that the quasiparticles are weakly interacting.

The $\alpha(\rho)$ coefficients we have extracted from these results for the three densities are $0.37(5), 1.01(5)$, and $1.84(9)$ MeV, respectively. In Fig. 1 we show the energy per particle at different densities versus polarization. To facilitate comparison between results at different densities we have divided the energy per particle with the energy of a free Fermi gas at the same total density:

$$E_{FG} = \frac{3}{10}\frac{\hbar^2}{m}(3\pi^2\rho)^{2/3} . \qquad (23)$$

We notice that, just like in the case of unpolarized neutron matter [34], when the density increases the energy in units of E_{FG} drops, but the rate of the drop is also decreasing. The slight deviation from linear behavior at ρ_1 stems from the afore-mentioned necessity to propagate up to longer imaginary times (at least by a factor of 3) in comparison to the other cases. This is also the reason why the results for the bigger systems at that density have larger error bars.

Further results for the energy of polarized neutron matter are given in Table I. Table I refers to the largest density we have studied, $\rho_3 = 5.32 \times 10^{-3}$ fm^{-3}. At this density we find the maximum value of the same-spin perturbative correction, which is 9 percent of the total energy. As should be expected, for the $33 + 33$ system the energies of the $\uparrow\uparrow$ and the $\downarrow\downarrow$ interactions are identical (within statistical error). As we increase the polarization, there is a clear trend toward the increase of the $\uparrow\uparrow$ rel-
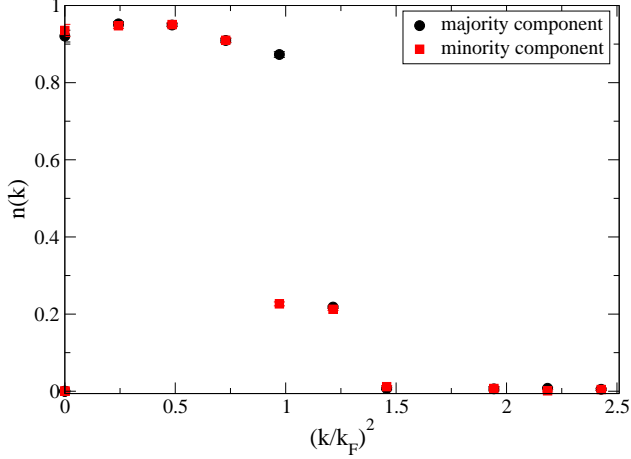
FIG. 2: (color online) Momentum distribution versus $(k/k_F)^2$ for the two different spins, for the case of 37 $\uparrow$ and 33 $\downarrow$ particles (total density $\rho_3 = 5.32 \times 10^{-3}$ fm^{-3}), shown as circles and squares respectively. k_F is taken here to refer to the total density, $k_F = \left(3\pi^2 \rho_3\right)^{1/3}$. The behavior exhibited is commonly referred to as "Fermi surface mismatch".
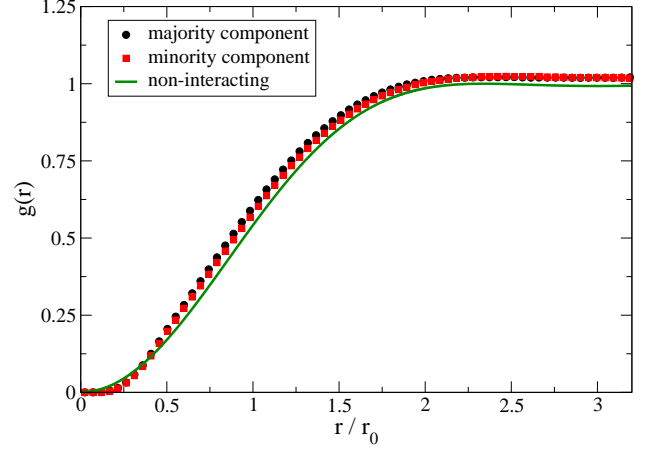

FIG. 3: (color online) Same-spin pair-distribution function as a function of the distance divided with a measure of the average interparticle distance, for the case of 37 $\uparrow$ and 33 $\downarrow$ particles (total density $\rho_3 = 5.32 \times 10^{-3}$ fm^{-3}), shown as circles and squares respectively. Also given is the same-spin pair-distribution function for a non-interacting Fermi gas (line).

ative importance, which becomes nearly double that of the corresponding $\downarrow\downarrow$ energy for the 43+33 system. In all cases, the same-spin contribution to the energy is small, not growing to more than 1 percent of the total energy.

B. Distribution functions

We have also used GFMC to calculate distribution functions at $\rho_3 = 5.32 \times 10^{-3}$ fm^{-3} for 37 $\uparrow$ and 33 $\downarrow$ particles: in contradistinction to the case of the energy, the results for these functions are not upper bounds to the true ground-state results, but they are expected to be accurate (the error being of second order in $|\Psi_0 - \Psi_V|$).

Starting with the momentum distribution, we first discuss our expectations using mean-field BCS theory as a guide. BCS is not quantitatively accurate in this regime, [34] but can provide qualitative understanding. In BCS, the momentum distribution is given by the following expression:

$$n(\mathbf{k}) = \frac{1}{2}\left[1 - \frac{\xi(\mathbf{k})}{E(\mathbf{k})}\right] , \qquad (24)$$

where $\xi(\mathbf{k}) = \epsilon(\mathbf{k}) - \mu$, the chemical potential is μ and $\epsilon(\mathbf{k}) = \frac{\hbar^2 k^2}{2m}$ is the single-particle energy of a particle with momentum $\mathbf{k}$. The elementary quasi-particle excitations of the system have energy:

$$E(\mathbf{k}) = \sqrt{\xi(\mathbf{k})^2 + \Delta(\mathbf{k})^2} \qquad (25)$$

Overall, this is close to a step function for small gaps, but it changes considerably in the strong coupling regime. In

general, the spread of the momentum distribution around μ is approximately 2Δ. At this density, the system exhibits a gap of $\Delta = 1.05(11)$ which as a fraction of the Fermi energy is $\Delta/E_F = 0.17(2)$ implying that there is no clearly defined Fermi surface. [34] Even so, in the case of spin-polarized Fermi gases it is customary to use the language of weak coupling and speak of a "Fermi surface mismatch". This follows from the fact that the Fermi energy is proportional to $\rho_{\uparrow(\downarrow)}^{2/3}$ and in this case the densities for the two spin populations are different.

In Fig. 2 we show the momentum distribution computed using GFMC. This is calculated as the Fourier transform of the one-body density matrix, through:

$$n_{\uparrow(\downarrow)}(k) \equiv \frac{N_{\uparrow(\downarrow)}}{L^3}\left\{\int d\delta r e^{i\mathbf{k}\cdot(\mathbf{r}'_n - \mathbf{r}_n)}\frac{\Psi_V(\mathbf{r}_1, \ldots, \mathbf{r}'_n)}{\Psi_V(\mathbf{r}_1, \ldots, \mathbf{r}_n)}\right\} , \qquad (26)$$

where the curly brackets denote a stochastic integration over the angles. The integral over $\delta r = |\mathbf{r}'_n - \mathbf{r}_n|$ is performed on a line analytically to avoid statistical errors due to the oscillatory radial dependence. In both cases, we see a considerable spread around the chemical potential value, but we also notice a clear distinction in how the two species behave around that point, the majority species showing a "lag" in its decline.

We have also computed the pair-distribution functions and have plotted them in Fig. 3. These are calculated from an expectation value of the form:

$$g_P(r) = A\sum_{i<j}\langle\Psi_0|\delta(r_{ij} - r)O_{ij}^P|\Psi_V\rangle , \qquad (27)$$

where we are interested in the case in which the operator is simply unity, and the normalization factor A is

such that $g_1(r) \equiv g_c(r)$ goes to one at large distances. Such pair-distribution functions provide sum rules related to density- and other response functions versus density and momentum. The solid line in the figure shows the pair-distribution function of noninteracting (NI) fermions with parallel spins:

$$g_c^{NI}(r) = 1 - \frac{9}{(k_F r)^6} \left[\sin(k_F r) - k_F r \cos(k_F r) \right]^2 \ . \quad (28)$$

The x-axis is the interparticle distance divided with a quantity, r_0, which describes the average interparticle spacing:

$$\frac{4}{3}\pi r_0^3 = \frac{1}{\rho} \ . \quad (29)$$

The free Fermi gas result is close to but distinct from both QMC results (for spin-up and spin-down particles) due to the effect of the interactions. As is to be expected, the majority component values are slightly larger than those of the minority species, implying that it is slightly more likely to find a spin-up particle than a spin-down one.

IV. CONCLUSIONS AND FUTURE WORK

In summary, we have studied superfluid spin-polarized low-density neutron matter at small polarizations using a variationally optimized approach that includes the dominant well-known terms in the Hamiltonian. We have calculated the equation of state with the AV4′ interaction at different densities. We have also calculated the momentum and pair-distribution functions for low-density neutron matter. We find clear signals of a Fermi surface mismatch, as expected, and also a linear dependence of the energy on the polarization. These results are in principle relevant to the physics of magnetars. Furthermore, they could be tested directly by using ultracold fermionic atom gases with unequal spin populations. In the case of cold atoms, Quantum Monte Carlo simulations of spin-polarized matter have been used as input to

density-functional theory approaches.[41, 42] Thus, our corresponding results for neutron matter might also be used as input to self-consistent mean-field models of nuclei.

This line of Quantum Monte Carlo calculations, having first been applied to and verified in cold atomic experiments, can also provide directions for future work in the field of nucleonic infinite matter. The simplest case is that of a two-component gas where the two populations are equal.[33, 34] The next step is to examine the ramifications of taking different populations for the two components: this is the case of spin-polarized low-density neutron studied in this work. Cold-atom experiments have by now also addressed Efimov physics, in which three components are involved. In the nuclear context, adding a third species could provide further insight into the physics of neutron stars. If the third component particles were taken to be protons and, as in this paper, only a few of them were added, then it would be possible to study highly asymmetric nuclear matter. Another possible avenue of future research is related to optical lattice experiments with cold atoms: to first approximation these are equivalent to periodic external potentials. In the nuclear case, an external potential would allow us to study the static response of neutron matter and would also facilitate the understanding of the impact on neutron pairing of the ion lattice that exists in a neutron star crust.

[1] D. Page, J. M. Lattimer, M. Prakash, and A. W. Steiner, Astrophys. J. **707**, 1131 (2009).

[2] D. N. Aguilera, V. Cirigliano, J. A. Pons, S. Reddy, and R. Sharma, Phys. Rev. Lett. **102**, 091101 (2009).

[3] F. J. Fattoyev and J. Piekarewicz, Phys. Rev. C. **82**, 025810 (2010).

[4] N. Chamel, S. Goriely, and J.M. Pearson, Nucl. Phys. **A812**, 72 (2008).

[5] B. Friedman and V. R. Pandharipande, Nucl. Phys. **A361**, 502 (1981).

[6] A. Akmal, V. R. Pandharipande, and D. G. Ravenhall, Phys. Rev. C **58**, 1804 (1998).

[7] J. Carlson, J. Morales, Jr., V. R. Pandharipande, and D. G. Ravenhall, Phys. Rev. C **68**, 025802 (2003).

[8] A. Schwenk and C. J. Pethick, Phys. Rev. Lett. **95**, 160401 (2005).

[9] J. Margueron, E. van Dalen and C. Fuchs, Phys. Rev. C **76**, 034309 (2007).

[10] M. Baldo and C. Maieron, Phys. Rev. C **77**, 015801 (2008).

[11] E. Epelbaum, H. Krebs, D. Lee, and U. -G. Meissner, Eur. Phys. J. A **40**, 199 (2009).

[12] E. Epelbaum, H.-W. Hammer, and U. -G. Meissner, Rev. Mod. Phys. **81**, 1773 (2009).

[13] T. Abe and R. Seki, Phys. Rev. C **79**, 054002 (2009).

[14] S. Gandolfi, A. Yu. Illarionov, F. Pederiva, K. E. Schmidt, and S. Fantoni, Phys. Rev. C **80**, 045802 (2009).

[15] A. Rios, A. Polls, and I. Vidaña, Phys. Rev. C **79**, 025802

(2009).

[16] K. Hebeler and A. Schwenk, Phys. Rev. C **82**, 014314 (2010).

[17] L. Luo and J. E. Thomas, J. Low Temp. Phys. **154**, 1 (2009).

[18] N. Navon, S. Nascimbène, F. Chevy, and C. Salomon, Science **328**, 729 (2010).

[19] J. Carlson and S. Reddy, Phys. Rev. Lett. **100**, 150403 (2008).

[20] A. Schirotzek, Y. I. Shin, C. H. Schunck, and W. Ketterle, Phys. Rev. Lett. **101**, 140403 (2008).

[21] B. Marcelis, B. Verhaar, and S. Kokkelmans, Phys. Rev. Lett. **100**, 153201 (2008).

[22] P. Haensel, Phys. Rev. C **11**, 1822 (1975).

[23] S. Fantoni, A. Sarsa, and K. E. Schmidt, Phys. Rev. Lett. **87**, 181101 (2001).

[24] I. Vidaña, A. Polls, and A. Ramos, Phys. Rev. C **65**, 035804 (2002).

[25] J. Marguergon, J. Navarro, and N. Van Giai, Phys. Rev. C **66**, 014303 (2002).

[26] A. Rios, A. Polls, and I.Vidaña, Phys. Rev. C **71**, 055802 (2005).

[27] G. H. Bordbar and M. Bigdeli, Phys. Rev. C **75**, 045804 (2007).

[28] F. Sammarruca and P. G. Krastev, Phys. Rev. C **75**, 034315 (2007).

[29] M. Ángeles Pérez-García, J. Navarro, and A. Polls, Phys. Rev. C **80**, 025802 (2009).

[30] J. Carlson and S. Reddy, Phys. Rev. Lett. **95**, 060401 (2005).

[31] S. Pilati and S. Giorgini, Phys. Rev. Lett. **100**, 030401 (2008).

[32] J. Carlson, S. Y. Chang, V. R. Pandharipande, and K. E. Schmidt, Phys. Rev. Lett. **91**, 050401 (2003).

[33] A. Gezerlis and J. Carlson, Phys. Rev. C **77**, 032801(R) (2008).

[34] A. Gezerlis and J. Carlson, Phys. Rev. C **81**, 025803 (2010).

[35] T. D. Lee and C. N. Yang, Phys. Rev. **105**, 1119 (1957).

[36] L. P. Gorkov and T. K. Melik-Barkhudarov, JETP, **40**, 1452 (1961) [Soviet Phys. JETP **13**, 1018 (1961)].

[37] R. B. Wiringa, V. G. J. Stoks, and R. Schiavilla, Phys. Rev. C **51**, 38 (1995).

[38] R. B. Wiringa and S. C. Pieper, Phys. Rev. Lett. **89**, 182501 (2002).

[39] J. P. Bouchaud, A. Georges, and C. Lhuillier, J. Phys. (Paris) **49**, 553 (1988).

[40] V. R. Pandharipande and H. A. Bethe, Phys. Rev. C **7**, 1312 (1973).

[41] A. Bulgac and M. M. Forbes, Phys. Rev. Lett. **101**, 215301 (2008).

[42] A. Bulgac, M. M. Forbes, and P. Magierski, arXiv:1008.3933, to appear in *BCS-BEC Crossover and the Unitary Fermi Gas*, edited by W. Zwerger, Lecture Notes in Physics (Springer, 2011).